Applied Physics A (2022) 128:508
https://doi.org/10.1007/s00339-022-05639-1

Applied Physics A
Materials Science & Processing

Effect of chromium-doping on structure and opto-electronics properties of nanostructured indium tin oxide thin films

Rashid Ali[1] · Muhammad Hanif[2] · Syed Abdul Basit Shah[1] · Syed Zameer Abbas[1] · Muhammad Ramzan Abdul Karim[1] · Muhammad Arshad[3] · Syed Haseeb Ali Ahmad[4]

Received: 8 November 2021 / Accepted: 25 April 2022 / Published online: 18 May 2022

Abstract

Indium-tin-oxide (ITO) thin films co-sputtered with chromium (Cr) have been studied for their structural, electrical, and optical properties. The fabrication has been carried out at room temperature in oxygen-deficient environment under different sputtering power on chromium target followed by thermal annealing in air at 300 °C for 1 h. Experimental characterizations reveal a decrease in grain, crystallite size, increase in crystallinity, and major diffraction peak (222) shift towards higher angle with increase in Cr-doping content. XPS spectra confirmed the presence of Cr as Cr^{3+}, Cr^{6+}oxidation state, and oxygen vacancies in Cr-doped ITO thin films. The presence of more structural defects due to difference in ionic radii between dopant (Cr^{3+} and Cr^{6+}) and host ions (In^{3+}), consequently, increases the carrier concentration. The decrease in carrier mobility (≈ 18%) is caused by the disordering related to increase in Cr content and decreased crystallite size that favor surface trapping states. UV–Vis spectroscopy showed that ITO thin film having thickness of 300 nm doped with ≈ 1 at. % Cr content has optimum opto-electronic properties, an average transmittance of ≈ 86% in the visible range (380–780 nm), and band gap of 3.82 eV. For the same Cr-doping, four-point probe investigation indicates resistivity of 7.65×10^{-5} Ω.cm, carrier density 2.2×10^{21} cm^{-3}, and carrier mobility of 36.7 cm^2 $V^{-1}S^{-1}$. The significant decrease in resistivity of approximately nine times in produced thin films compared with relevant work in literature is the combined effect of Cr-doping and annealing which affect the carrier density and crystallinity.

Keywords Magnetron co-sputtering · Chromium-doped indium tin oxide (ITO) · Transparent electrode · Post-annealing in air · Carrier concentration

1 Introduction

Indium tin oxide (ITO) has numerous applications due to its unique properties, including electrical conductivity, optical transparency, and ease to deposit as thin films. Transparent indium tin oxide as thin films is used for the anode of organic light-emitting diodes [1], solar cells [2], aircraft windshield [3], liquid crystal display [4], touch panel [5], and various other electronic applications [6, 7]. With such a breadth of ITO applications, researchers have been striving to improve opto-electronic properties in a cost-effective manner. Several studies reported the effect of various dopants on structural, electrical, and optical properties of indium tin oxide thin films based on content of dopant, their oxidation state, higher carrier mobility, and ionic radius difference with the host material. Doping with transition elements such as Cr [8], Mo [9], Ti [10], Ni [11], Zr [12], and Ag [13] etc. can improve opto-electronic properties as a result of smaller ionic radius, higher charge carrier mobility, and difference in oxidation state. Since, the possible existence of Cr in multiple stable charge states as Cr^{3+} and Cr^{6+} [8] and smaller ionic radii compared to In^{+3} can considerably decrease the resistivity with moderate doping concentration. Moreover, high chromium-doped indium oxide (Cr-IO) [14]

✉ Rashid Ali
rashidali@giki.edu.pk

[1] Faculty of Materials and Chemical Engineering, Ghulam Ishaq Khan Institute of Engineering Sciences and Technology, Topi, Swabi, KPK, Pakistan

[2] School of Photovoltaics and Renewable Energy Engineering, University of New South Wales (UNSW), Sydney, Australia

[3] Nanoscience and Technology Division, National Center for Physics, Quaid-I-Azam University, Islamabad, Pakistan

[4] School of Chemical Engineering, University of Queensland, Brisbane, Australia

and indium tin oxide (Cr-ITO) [15] thin films produced in oxygen-deficient environment form Cr-oxygen vacancy complexes which caused carrier-controlled ferromagnetism. The oxygen vacancies provide mobile charges and contribute to form the magnetic building block whose polarized states can be occupied by extrinsic charge, provided by dopants or vacancies in excess over the dopant concentration. The combination of transparency, electrical conductivity, and magnetic behavior in addition to chemical stability makes the Cr-doped ITO a viable candidate to study.

In this connection, there are studies on preparation of Cr-doped ITO thin films using various deposition techniques such as magnetron co-sputtering [16], pulsed laser deposition [17], and sol–gel process [8]. Indeed, several different results are reported while attempting to address the contribution of Cr-doping to ITO thin-film properties. The improvements in opto-electronic properties are related to the microstructure, morphology, and structure features evolution in ITO caused by different deposition conditions, thin-film thickness, Cr dopant content, and its charge state. The increase in Cr-doping causes structural disorder in ITO that leads to decrease in carrier concentration, carrier mobility, and increase in resistivity. The low Cr-doping narrows the optical band gap due to shallow and deep energy levels stemming from dopant, while high Cr-doping widens the gap due to structural disorder by the shrinkage in lattice parameters and doping-induced strains [17]. In as-deposited thin films at room temperature, the Cr-doping and film thickness above critical value impart crystallinity which increases the carrier concentration but reduce the mobility due to doping-induced disorder [16]. The room-temperature growth by co-sputtering implies disordering, lower crystallinities, and stresses that require thermal annealing. Also, the Sn and Cr in ITO do not contribute to free carrier as these have to be thermally activated to substitute for In and contribute to free carriers in the matrix. However, post-annealing in oxidized environment increases the dopant charge state from Cr^{3+} to Cr^{6+} and improves the structural disorder, causing increase in carrier concentration, carrier mobility, and optical band gap of ITO thin films [8]. The possible difference in properties of Cr-doped ITO thin films could be due to different oxidation conditions of produced films.

Most of studies deposited Cr-doped ITO thin films in oxygen environment; nevertheless, less attention has been paid to study in the oxygen-deficit environment followed by thermal annealing. The high concentration of oxygen vacancies in thin films produced in argon atmosphere can cause high carrier mobility and lowest optical properties [18]. The carrier concentration and mobilities of ITO increased up to process temperature of 300 °C beyond which mobility starts to decrease as a result of ionized impurity scattering [19]. Moreover, annealing in air rather than in oxygen atmosphere is expected to impact on the final content of oxygen vacancies [20, 21]. In fact, a procedure for the development of Cr-doped ITO thin films with reproducible and optimal properties is yet to be reached. The present study, therefore, sought to report the structural, morphological, electrical, and optical properties of Cr-doped ITO thin films having thickness of 300 nm deposited in oxygen-deficit environment followed by post-annealing treatment in air at 300 °C.

2 Experimental procedure

2.1 Cr-ITO thin-film preparation

Chromium-doped indium tin oxide (Cr-ITO) thin films were deposited on glass substrates using Ollital multi-target RF-DC magnetron co-sputtering equipment. Indium tin oxide (In_2O_3 and SnO_2 in a weight ratio of 9:1) and Cr having a purity of 99.995% and diameter of 50 mm were used as sputtering targets, on direct current (DC) and radio frequency (RF), respectively. Ultrahigh purity argon gas (99.999%) was used as sputtering gas at a constant flow rate of 70 SCCM. Before deposition, the substrates were cleaned in an acetone bath and with argon plasma at 400 V bias voltage for 5 min.

The sputtering targets (ITO and Cr) were pre-sputtered on shutter to eliminate any impurity on the surface of the targets. The chamber was evacuated to a base pressure of 3.2 mPa for each deposition while maintaining a working pressure of 400 mPa. The target-to-substrate distance was 60 mm, and substrate rotation was employed to keep the thin-film thickness uniform and facilitate co-sputtering. The Cr-doped ITO thin films were produced by keeping the ITO on DC power (90 W) while varying the RF power (0, 20, 30 and 40 watts) on the chromium target. In-situ thickness was monitored with quartz crystal and was maintained at $\approx 300 \pm 5$ nm for all thin films. When the film reaches the pre-programmed thickness value, the shutter located in front of target automatically closes. The produced thin films were thermal annealed at 300 °C for 1 h in the air atmosphere and then furnace cooled in Samlab SX2-3-18TP electric furnace.

2.2 Characterizations

The stoichiometry and structural properties of produced thin films were studied using X-ray diffraction (XRD) with Empyrean Panalytical X-ray diffraction system in Bragg–Brentano (θ–2θ) scan mode using monochromatic Cu-Kα (1.54 Å) radiation source with an accelerating voltage of 40 kV and tube current of 25 mA at room temperature. The goniometer scanned at 0.002° for peak resolution from 2θ of 28° to 32°. The crystallite size is determined with a precision of ± 2 nm, using Scherrer's equation [Eq. (1)]

$$D = \frac{0.9\lambda}{\beta \cos\theta} \quad (1)$$

where D, λ, β, and θ correspond in turns crystallite size, the wavelength of the X-ray source, full width half maximum (FHWM), and peak position of X-ray diffractogram.

The surface morphology, surface roughness over a fixed 1 μm^2 area of the sample, and grain size are investigated using an atomic force microscope in tapping mode by Nanosurf AFM. The ultraviolet–visible spectroscopy using Perkin/Elmer 1500 is performed to evaluate thin-film transmittance, reflectance, and absorbance over the wavelength range from 200 to 1000 nm. Four-point probes resistivity and Hall measurement are carried out using the Hall-8800 model apparatus manufactured by Nanomat. The carrier concentration and mobility of the films are measured by the Hall Effect in the van der Pauw configuration. Van der Pauw mode includes electrical measurements from the four corners of the square-shaped sample under an externally applied magnetic field. Five hall measurement readings were recorded for each sample to ensure the reproducibility of the results. To determine the charge state of each element in thin films, X-ray photoelectron spectroscopy (XPS) of thin films was conducted using Kratos Axis Ultra XPS instrument equipped with a monochromatic Al–K_α (1486.6 eV) X-ray source. The X-ray source was operated at 150 W at constant analyzer energy (CAE) 160 eV for survey scans, and 40 eV for detailed scans. The data acquisition with Kartos Vision software, and data analysis was performed with Igor pro along with XPS fit procedures. The curve fitting of spectra was achieved using Gaussian–Lorentzian line shape after performing the Shrilly background corrections. The XPS data are referenced with C1s at 284.4 eV for binding energy.

3 Results and discussion

3.1 Structural and microstructural characterization

The X-ray diffractograms of thin films in the annealed and unannealed conditions are shown in Fig. 1a. The as-deposited thin film at room temperature reveals a hump at $2\theta = 33°$ which indicates the deposition temperature lower than 100 °C, confirming the amorphous structure of indium [22]. However, after annealing for 1 h at 300 °C in the air, thin films show a major diffraction peak at (222) plane and the secondary planes (400), (411), (440), (211), and (622), which perfectly match with the ICDD database of indium oxide (PDF # 06–0416) and corresponds to reported in the literature on ITO thin films [21]. Indeed, the occurrence of the major diffraction peak (222) indicates the formation of indium oxide polycrystallites favored by annealing and Cr dopant acting as a nucleation seed. The oxygen vacancies are structural defects in indium oxide and manifest through the presence of (400) peaks in XRD diffractogram. The indication of very weak diffraction peak (321) at 2θ of ≈ 33°, which corresponds to metallic indium, is completely converted into indium oxide. No detectable X-ray diffraction peaks corresponding to Cr oxides or Cr are observed as the doping level is low.

The diffraction peak of indium oxide (222) in the range of 30°–31° shifted towards higher angle, and peak height

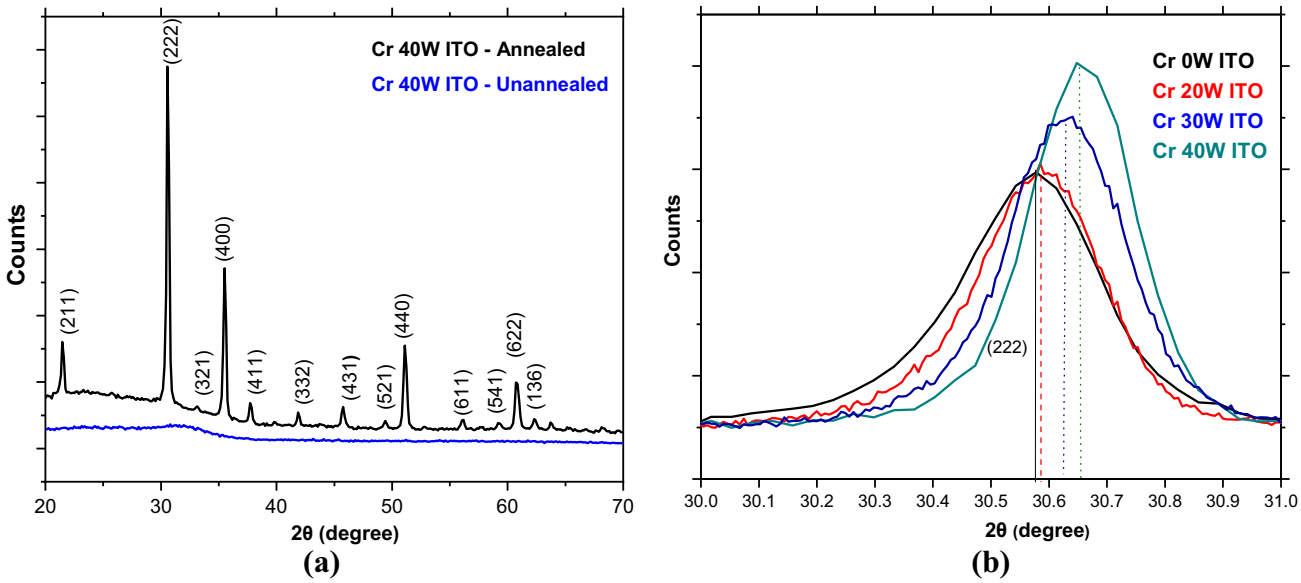

Fig. 1 X-ray diffraction pattern of: **a** Cr 40 W ITO thin films in annealed and as-deposited condition and **b** ITO (0 W Cr) in comparison with Cr-doped ITO under varying sputtering power on Cr target (20 W, 30 W and 40 W) thin films showing major peak (222) shifting to the right

increased with increase in sputtering power on Cr target (Fig. 1b). The possibility of peak shift towards higher angle can be due to ion-peening effect of different sputtering power on Cr target, thermal stresses [23], and Cr-doping. However, the possibility of ion-peening and thermal stresses is primarily eliminated because of post-deposition thermal annealing. Since only Cr content was varied and Sn contents in ITO target were fixed, therefore, the peak shift towards higher angle with increase in sputtering power on Cr target is due to Cr-doping content. This is because the Cr^{3+} and Cr^{6+}, potential dopants, have smaller ionic radii of 0.63 Å and 0.44 Å, respectively, compared to 0.94 Å for In^{3+} [24]. The substitution of In^{3+} by the smaller Cr cations (Cr^{3+} or Cr^{6+}) in the crystal lattice sites could decrease the final distance between Cr and their oxygen neighbors, causing dopant-induced strains [25]. The lattice contraction and decrease in lattice constants is expected upon relieving of the dopant-induced strains. The dopant-induced strain increases with an increase in film thickness, and the film becomes unstable beyond critical film thickness, causing strain relaxation. The post-annealing and significant thickness of thin film (300 nm) both helped to relieve the dopant-induced elastic strain energy, leading to change in lattice parameters. The shift in major diffraction peak (222) towards higher angle [26] and increase in peak height with increase in sputtering power on Cr target caused the decrease in lattice constants. Table 1 summarizes the structural parameters calculated for major diffraction peak (222) of ITO, AFM measured average grain size, roughness, and FESEM-EDX atomic composition of produced thin films.

The trend in peak shift is in agreement with the study [14] in which 4 at.% Cr-doping content in indium oxide thin films causes the peak shift towards a higher angle and decreases lattice constant from 10.114 Å (un-doped) to 10.075 Å. The decrease in lattice constants provides the evidence that Cr atoms substitute into In sites. The increase in X-ray diffraction peak intensity with increased sputtering power on Cr target (Cr 30 W and Cr 40 W) also corresponds to a smaller crystallite size and more crystalline structure. A significant decrease in crystallite size is seen in FESEM micrographs (Fig. 2) as well as in X-ray diffraction analysis (Table 1) for Cr 40 W compared with Cr 0 W ITO thin films.

The uniformity in thin-film composition was assessed using multiple FESEM-EDX measurements at different sample positions at 15 kev with 9000 counts to get complete thin-film information. All spectra showed a minimal difference in In, Sn and Cr composition in all these regions, showing the uniformity of Cr dopant distribution in thin

Table 1 XRD structural parameters, FESEM-EDX measured Cr content and AFM average grain size under different sputtering power on Cr target

Cr power (W): ITO	2θ (°)	Lattice constant (Å)	XRD crystallite size (nm)	Cr (at.%)	AFM average grain size (nm)	RMS Roughness (nm)
Cr 0 W	30.571	10.121	50	0	56.2	0.59
Cr 20 W	30.584	10.117	49	0.5	49.1	0.47
Cr 30 W	30.625	10.104	34	1	45.4	0.38
Cr 40 W	30.655	10.094	22	1.9	37.5	0.27

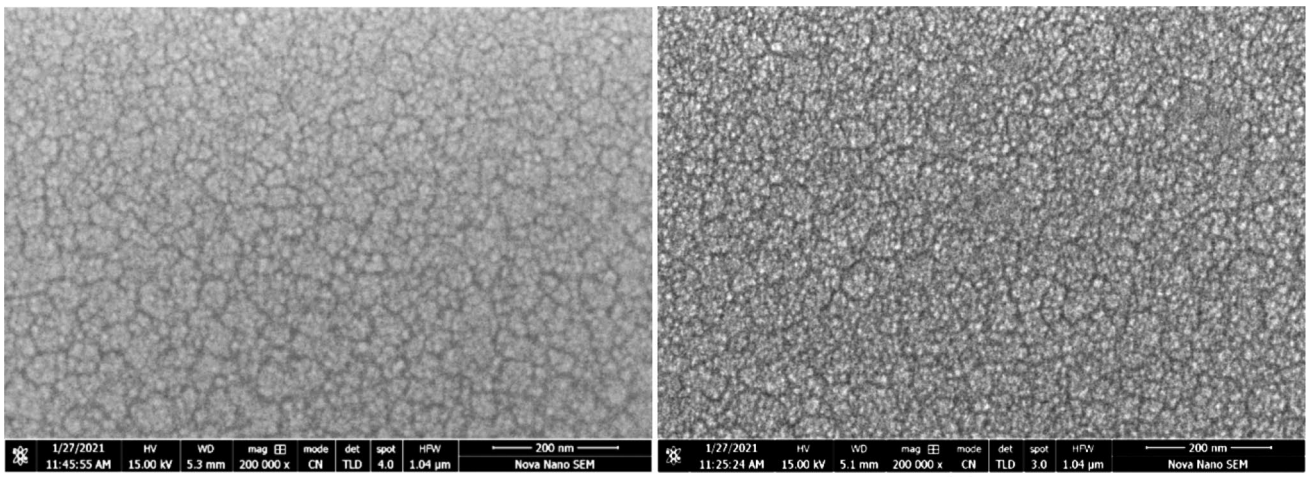

Fig. 2 FESEM micrographs at same magnification of annealed: **a** Cr 0 W ITO thin film and **b** Cr 40 W ITO thin films having 1.9 at.% Cr content

films. With the increase in sputtering power on Cr target from 20 to 40 W, the chromium-doping content of films is increased from 0.5 to 1.9 at.%, respectively, as measured by FESEM-EDX analysis.

The average grain size of as-deposited ITO thin films was found to be ≈ 30 nm. However, a slight decrease in grain size of ≈ 5 nm was found for Cr 40 W. The thermal annealing significantly increases the grain size due to fusion of individual grains to form polycrystalline grains. However, the increase in grain size of Cr-doped ITO is lower than ITO as Cr acts as nuclei of heterogeneous nucleation sites to create many crystallites of smaller size. The surface morphology of thin films in annealed condition was probed using an atomic force microscope, and Fig. 3 shows the two-dimensional (2-D) micrographs of ITO and Cr-doped ITO thin films.

The visual analysis of Cr-doped ITO thin-film AFM micrographs seems having larger grain size than ITO, which might be due to fusion of individual grains (Fig. 3a, b). However, after analyzing the grains with the Gwydion software line scan option, multiple grains are found within the curved domed grains. Figure 4 shows the AFM image together with surface line profile analysis of 0.5 at. % Cr-doped ITO thin films.

The width of oscillation in line profile was used to find the size of the grains (4b). The presence of smaller grains of several tens of nanometers within larger grains is evident from the AFM line profile (Fig. 4b), appearing as small-amplitude oscillations within larger grain [27]. The surface morphology of thin films exhibited as tightly packed grains. The noticeable decrease in grain size can be clearly seen in ITO thin film doped at sputtering power on Cr target 30 W and 40 W (Fig. 3c, d). The nucleation on the surface might be responsible for the formation of smaller grains within large grains. The Cr-doping causes the creation of nucleation sites and an increase in interfacial energy, which hinders the further crystal growth. To overcome this, particle clustering reduces the interfacial energy marked by a decrease in average grain size [28]. The Cr-doped ITO thin films also exhibited curved grain boundaries and alignment in grain along with the difference in amplitudes. According to studies in the literature, the decrease in grain size and alignment in grains (which might indicate grain fusion) is found with an increase in Cr content in ITO thin films [8, 29]. This grain morphology could be due to the lattice strain caused by dopant concentration as the difference in lattice parameters and peak shift observed in X-ray diffraction analysis. The noticeable increase in pores and voids in thin films could be due to incorporation of sputtering gas (argon) and an increase in number of vacancies [30]. The decrease in AFM grain size and increase of crystallinity in Cr-doped ITO thin films are also in line with the reduction in XRD crystallite size and increased crystallinity (Cr 30 W and Cr 40 W). The decrease in grain size with Cr-doping corresponds to

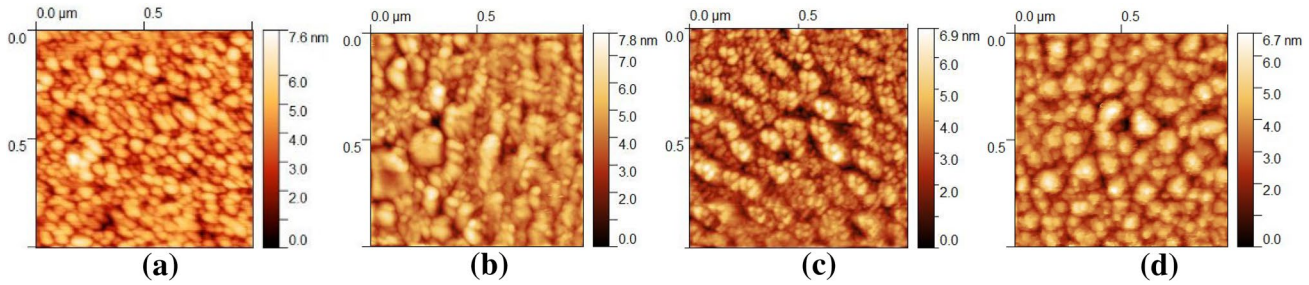

Fig. 3 AFM two-dimensional images of ITO and Cr-doped ITO thin film after thermal annealing (size 1 µm × 1 µm): **a** Cr 0 W; **b** Cr 20 W; **c** Cr 30 W and **d** Cr 40 W

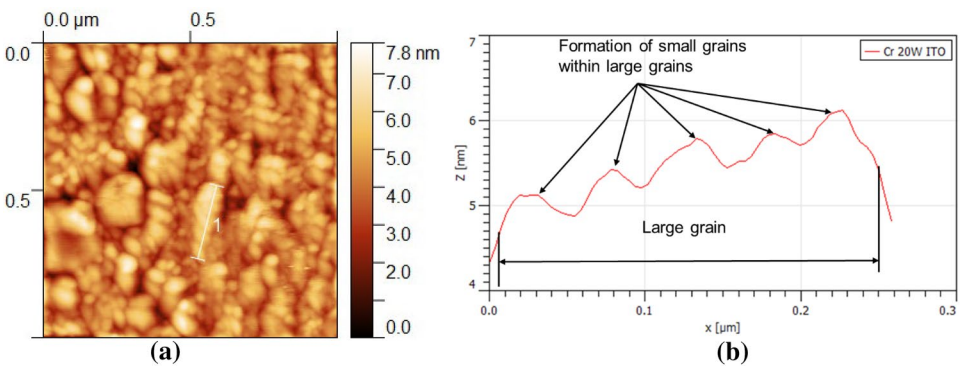

Fig. 4 Atomic force microscopy (AFM) image and line profile across the thin-film surface: **a** A two-dimensional image of 0.5 at. % Cr-doped ITO thin films and **b** line profile across the selected line in AFM image

a slight reduction in average surface roughness of 0.27 nm, as shown in Table 1 [16]. Figure 5 shows the histograms of average grain size analysis by precisely measuring the distribution of visible grains from the line scan profile of the two-dimensional AFM image.

The grains with size < 30 nm (Fig. 5a) are individual grains; however, the grains of the same size range in the histograms of Fig. 5b–d are smaller grains due to the nucleation process as demonstrated through line scan in Fig. 4b. The AFM measured average grain size is 6–8 nm higher than obtained from the XRD major peak (222) using Scherrer's equation.

3.2 Surface elemental characterizations

The bonding state of ITO thin films doped with 1.9 at. % of Cr is measured using XPS, and results are shown in Fig. 6.

The In 3*d* spectra (Fig. 6a) are resolved into two components, at 444.8 eV and 452.3 eV corresponds to In-$3d_{5/2}$ and In-$3d_{3/2}$ transitions, respectively, which indicates the In^{3+} oxidation state and corroborates well with the ITO thin films in the literature [31]. In O1s spectra, the peak at 529.9 eV corresponds to the oxygen atoms surrounded by In, called as O_I, whereas the other component with binding energy of 531.18 eV, called as O_{II}, represents O^{2-} ions arising from oxygen-deficient regions, which can be attributed partly to the oxygen vacancies. Noticeably, the integrated areas of O_I and O_{II} components of O1S spectra for doped and undoped ITO thin film qualifies a sensitive indicator of the variation in oxygen vacancy concentration. The variation trend in oxygen vacancies concentration with Cr-doping can be attributed to the presence of more structural defects due to difference in ionic radii between the dopant (Cr^{3+} and Cr^{6+}) and host ions (In^{3+}). Since, one oxygen vacancy results in two electrons being released from covalent bonding with transition metals [18]. The Sn 3d spectra could be fitted at 486.75 eV and 495.6 eV for Sn-$3d_{5/2}$, Sn-$3d_{3/2}$, respectively (Fig. 6c). These assignments are associated with Sn^{4+}-binding state of tin. The high-resolution scan of Cr 2*p* shows doublet (Cr $2p_{3/2}$ and Cr $2p_{1/2}$) with asymmetrical peaks. The spectra appear at 576.83 eV and 586.2 eV for Cr $2p_{3/2}$ and Cr $2p_{1/2}$, corresponding to Cr^{3+} states of Cr atoms (Fig. 6d). The peaks appearing at a binding energy of 579.2 eV are related to Cr^{6+} cations and matches with the Cr-doped ITO thin films in the literature [8]. Indeed, post-annealing in air favors the oxidation of Cr^{3+} to Cr^{6+} by turning the commonly anticipated isovalent doping into heterovalent, causing remarkable structural changes and increase in carrier concentration. When, two Cr^{6+} ions substitute two In^{3+} ions, three oxygen vacancies are generated in the lattice for charge compensation. The two oxygen vacancies are compensated by formation of two-interstitial oxygen O_i'' anions vacancies which occupy some of the structural anion vacancy site of In_2O_3. Thus, two-interstitial oxygen (O_i) anions vacancies reduce the number of free carriers—from six to two. The remaining one vacancy contributes two free carriers in the lattice. The following Kröger–Vink notation [Eq. (2)] explains the mechanism of Cr^{6+} cations doping:

$$In_2O_3 + 2Cr \Rightarrow \left[2Cr_{In}^{\bullet\bullet\bullet} O_i''\right]^{\bullet\bullet} + 2e' + \frac{1}{2}O_{2(g)} \quad (2)$$

where the subscript stands for the site position and the superscript stands for effective negative (′) or positive (•) charge.

The post-annealing in oxidizing environment facilitates the formation of $\left[Cr_{In}^{\bullet\bullet\bullet} O_i''\right]^{\bullet}$ complexes given in Eq. 2.

3.3 Electrical properties

The evolution of electrical properties of the ITO thin films, such as resistivity, carrier density, and Hall mobility, as a function of sputtering power on Cr target is shown in Fig. 7.

The Cr-doping significantly increased the carrier concentration from 1.6×10^{21} (Cr 0 W) to 2.4×10^{21} cm^{-3} (Cr 40 W) but slightly decreased (≈ 18%) the carrier mobility from 42.7 (Cr 0 W) up to 35.1 $cm^2\ V^{-1}\ s^{-1}$ (Cr 30 W), and further, for Cr 40 W, there is not a notable change. The increase in carrier concentration is related to the electron donating mechanism of Cr^{6+} (Fig. 7) and reduced impact of trapping defect states due to improved crystallization and structure relaxation. The increase in crystallinity with Cr-doping

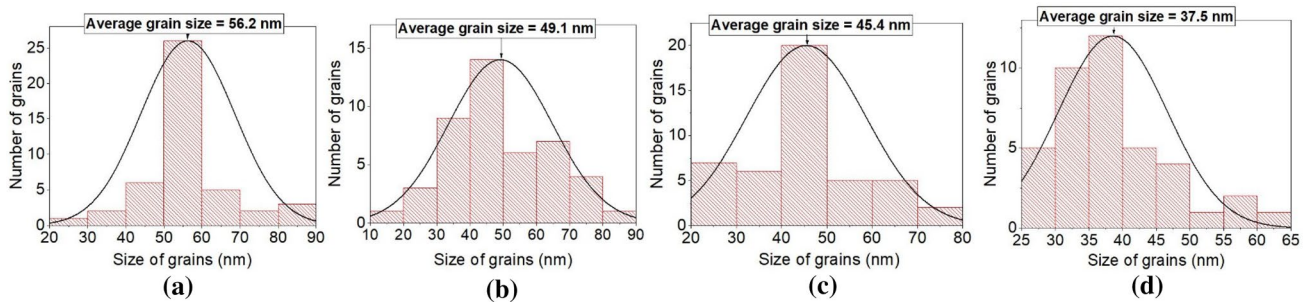

Fig. 5 Histograms displaying an average grain size of ITO and Cr-doped ITO thin film: **a** Cr 0 W; **b** Cr 20 W; **c** Cr 30 W; **d** Cr 40 W

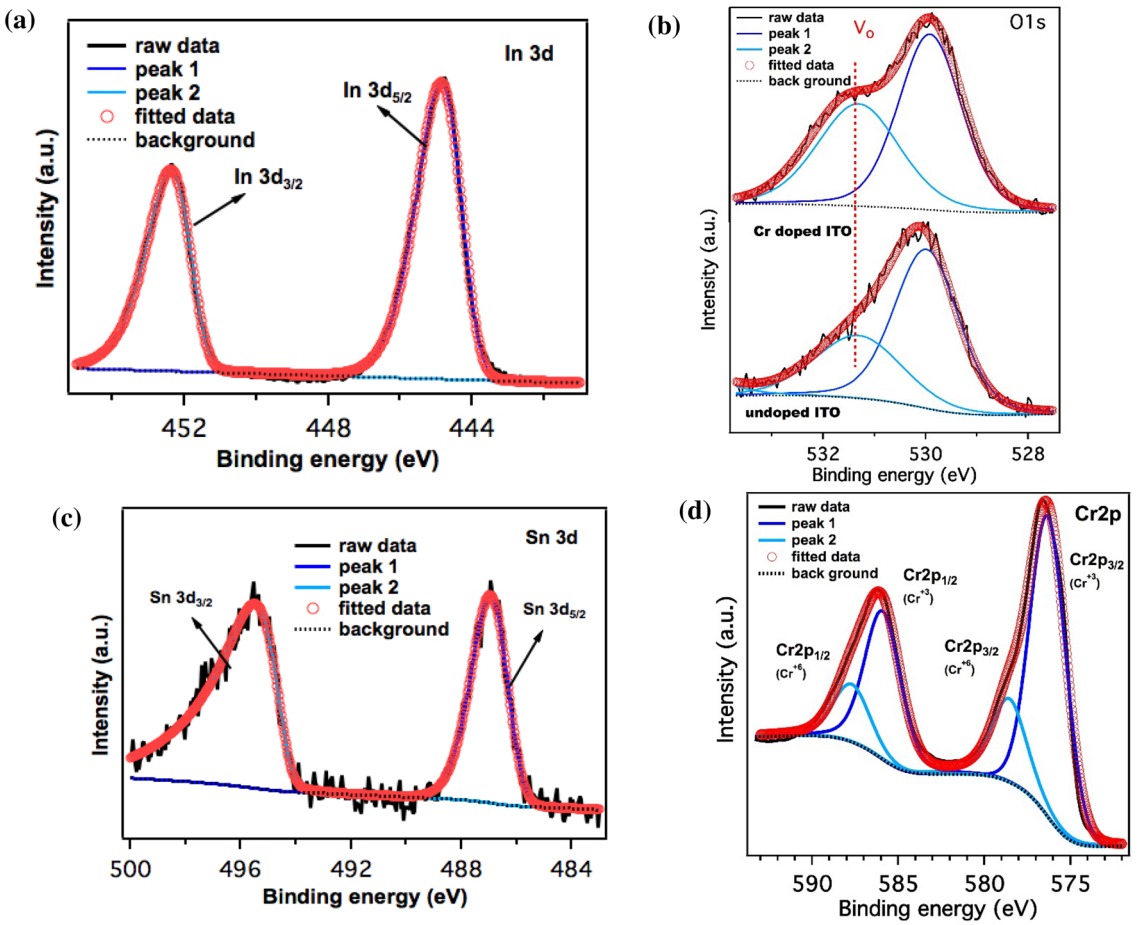

Fig. 6 XPS spectra for Cr-doped (1.9 at. %) ITO thin film thermal annealed at 300 °C: **a** In 3*d*, **b** O1S, **c** Sn 3*d*, and **d** Cr 2*p*

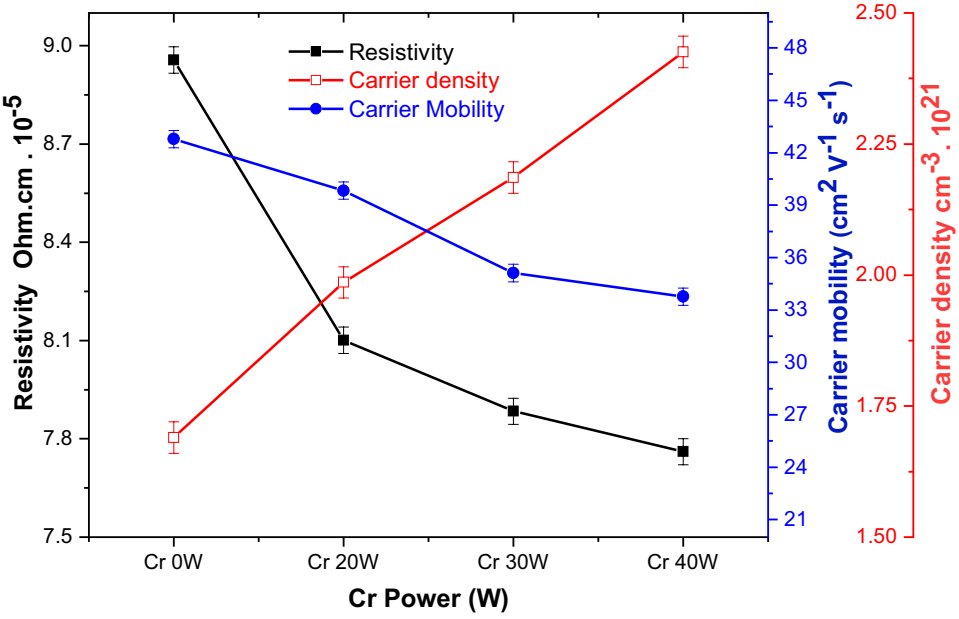

Fig. 7 Electrical properties of ITO thin film as a function of sputtering power on Cr target

content was confirmed from AFM and XRD data analysis. The decrease in carrier mobility can be explained based on lattice distortion due to relieve of elastic strain caused by Cr-doping and decreased crystallite size that favor surface trapping states. The slight decrease in crystallite size with increase in sputtering power on Cr target from Cr 0 W to Cr 20 W caused slight decrease in carrier mobility. However, significant drop in mobility from Cr 20 W to Cr 30 W could be due to abrupt change in crystallite size and Cr-induced lattice distortion. The change in mobility from Cr 30 W to Cr 40 W falls within margin of error which could be due to presences of interstitial anion vacancy which reduces the number of free carriers and improves the carrier mobility.

The overall effect of carrier concentration and mobility results decrease in resistivity value from 8.96×10^{-5} (Cr 0 W) to 7.6×10^{-5} Ω.cm (Cr 40 W). Previous reported literature on Cr-doped ITO thin films deposited by different processes shows resistivity values varying in the range of 10^{-1}–10^{-4} Ω.cm [17, 32] with lowest reported value of 7.3×10^{-4} Ω.cm having carrier concentration of 2.4×10^{20} cm^{-3} and mobility 27 cm^2 V^{-1} s^{-1} for Cr-doping content of 0.6 at. % in ITO thin films prepared at temperature lower than 100 °C by magnetron co-sputtering [16]. The significant decrease in resistivity of approximately nine times in our thin films compared with relevant work is the combined effect of Cr-doping and annealing which affect the carrier density and crystallinity.

3.4 Optical properties

The optical transmittance spectra and optical band gap of ITO and Cr-doped ITO thin films prepared under different sputtering power on Cr target followed by annealing in air are shown in Fig. 8a, b, respectively.

The fluctuations observed in the transmittance spectra are due to multiple-beam interference. The average transmittance for Cr 30 W ITO thin film is found around 86% at the wavelength from 400 to 800 nm and peak transmittance is increased up to ≈ 90% (Fig. 8a). The contributed factor behind the increase in optical transparency in visible range is ascribed to the increase in density of Cr^{3+}, Cr^{6+} carriers, decreasing the generation of black InO [33]. The lower impurity scattering due to lower size difference between ionic radii of Cr^{3+} (0.63 Å), Cr^{6+} (0.44 Å), and In^{3+} (0.94 Å) [8]. Beyond Cr 30 W, further increase in Cr-doping content (1.9 at. %) leads to slightly decrease in optical transparency due to more electron scattering by the larger grain boundaries and increase in lattice distortion. Moreover, noticeable shift in transmission-edge towards shorter wavelength for Cr 40 W ITO thin film is according to well-known Burstein–Moss or blue shift for doped semiconductors associated with increase in carrier concentration. The significant increase in optical absorption for Cr 30 W, which appears as interference maxima and minima in 350–700 nm spectral range of transmittance spectra, is influenced by the increased volume of crystallinity caused by Cr-doping [34]. In addition, enhanced crystallinity in Cr-doped ITO as compared to un-doped ITO is consistent with the steeper edge of transmittance curves (Fig. 8a), indicating Cr-induced crystallization [35]. The lower optical transmission (around 63%) of ITO thin film having 300 nm thickness could be ascribed to the formation of sub-stoichiometric indium oxide (InO) due to the formation of sub-stoichiometric indium oxide (InO) due to lower crystallization at the annealing temperature. The

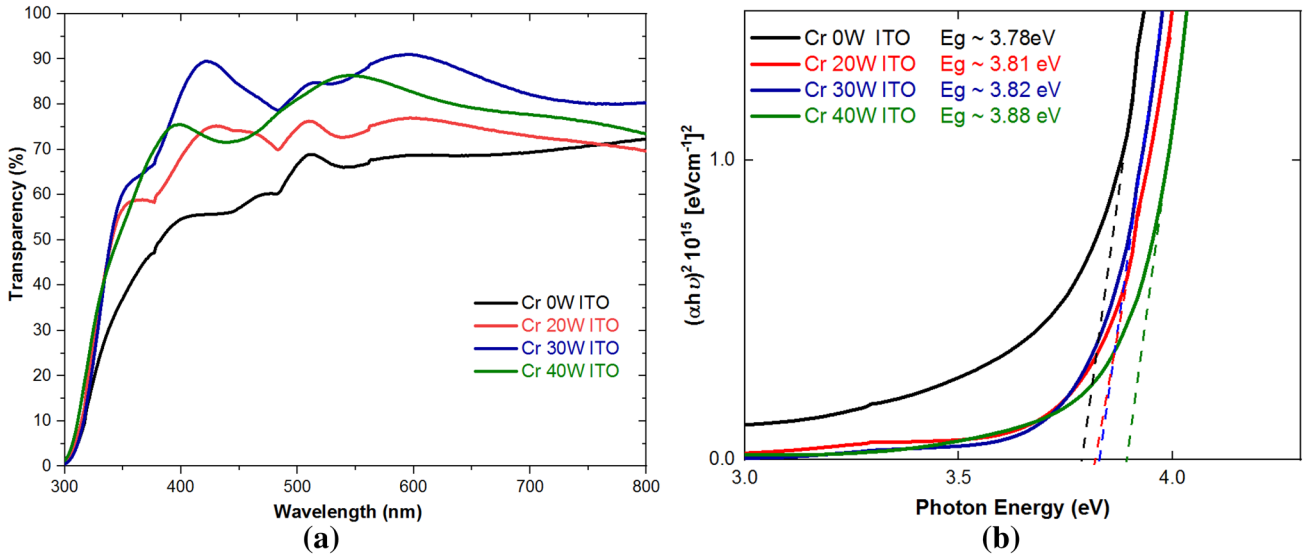

Fig. 8 **a** UV–visible optical transmittance of ITO thin film as a function of wavelength in the range of 300–800 nm for various sputtering power on Cr target. **b** Absorption coefficient versus photon energy for different sputtering power on Cr target. The dashed lines indicate linear extrapolations and x-intercept showing an estimated band gap

lower ITO crystallization was confirmed from the XRD as the lower intensity of diffraction peak (shown in Fig. 1) in comparison with Cr-doped ITO thin films.

To analyze the effect of band-edge on transparency, absorption energy for indirect allowed transitions $(\alpha h\nu)^2$ is plotted against the photon energy ($h\nu$) (Fig. 8b), where α is the absorption coefficient. A parabolic curve was obtained, and the band-gap values were calculated by extrapolating the linear part of the curve to the energy axis. The values of band gap obtained for un-doped, 0.5, 1, and 1.9 at. % Cr-doped ITO thin are 3.78, 3.81, 3.82, and 3.88 eV, respectively. The widening in optical band gap of ITO with increase in Cr-doping could be ascribed to lattice disorder due to decrease in lattice parameter by crystal re-structuring and increase in carrier concentration. The increase in carrier concentration with Cr-doping leads to filling the lowest energy states in the conduction band, thereby widening the band gap. The band-gap widening in Cr-40 W ITO thin films is due to the increase in the density of states in conduction band below the Fermi energy levels with the Cr-doping, which suggests the increase of carrier concentration. The increase in carrier concentration decreases the optical absorption owing to inter-band transition according to Burstein–Moss shift. Since, very small difference in band-gap values between Cr 20 W and Cr 30 W can also be ascribed to slightly different Fermi levels due to the better crystalline structure with increase in Cr content. However, higher absorption intensity and a longer tail of Cr 30 W compared with Cr 20 W (Fig. 8b) indicate dopant-induced disorder. The dopant-induced disorder caused the direct inter-band transitions from valence bands below the VBM at energies changing versus dopant concentration. The band-gap values reported in the literature for undoped 1.5, 2.0, and 2.5 at. % Cr-doped ITO thin films produced through sol–gel technique having (222) crystallographic growth were 3.25, 3.29, 3.42, and 3.06 eV, respectively [8]. In the present study, the difference in optical band-gap values between the un-doped and 1.9 at.% Cr-doped is 0.10 eV which is slightly lower than the value reported in the literature [8].

4 Conclusions

Chromium-doped indium-tin-oxide thin films are produced using the magnetron co-sputtering in oxygen-deficit environment followed by post-annealing treatment in air at 300 °C. The X-ray diffraction results show that as-deposited ITO and Cr-doped ITO thin films are amorphous-like. Characterizations reveal a decrease in grain size, crystallite size, and increase in crystallinity and major diffraction peak (222) shift towards higher angle with increase in Cr-doping content in ITO thin films. The Cr-doping causes the creation of nucleation sites and an increase in interfacial energy which hinders the further crystal growth. To overcome this, particle clustering reduces the interfacial energy marked by a decrease in grain size. The decrease in lattice parameters is related to lattice strain, increase in crystallinity caused by Cr-doping. The variation in oxygen vacancies concentration in Cr-doped ITO can be attributed to the presence of more structural defects due to difference in ionic radii between the dopant (Cr^{3+} and Cr^{6+}) and host ions (In^{3+}). The decrease in carrier mobility can be related to the lattice distortion with increase in Cr content and decreased crystallite size that favor surface trapping states. The Cr content of ≈ 1 at. % ITO thin film shows optimum opto-electronic properties, an average transmittance of ≈ 86% in the visible range (380–780 nm) with a band gap of 3.82 eV. For the same Cr-doping, four-point probe investigations indicate the resistivity of 7.6×10^{-5} Ω.cm, carrier density 2.2×10^{21} cm^{-3} and carrier mobility of 36.7 $cm^2\ V^{-1}S^{-1}$. Further increase in Cr-doping content of 1.9 at.%. caused scattering from the larger grain boundaries which slightly decreased the transparency.

Acknowledgements This research work is carried out through the financial support of the Higher Education Commission Islamabad, Pakistan under Project No: 10366/NRPU/R&D/HEC, to support research in universities and Ghulam Ishaq Khan Institute of Engineering Sciences and Technology, Topi, Pakistan.

References

1. Z. Chen et al., Highly ultraviolet transparent textured indium tin oxide thin films and the application in light emitting diodes. Appl. Phys. Lett. **110**(24), 242101 (2017)
2. M. Hösel et al., Fast inline roll-to-roll printing for indium-tin-oxide-free polymer solar cells using automatic registration. Energy Technol. **1**(1), 102–107 (2013)
3. J. Txintxurreta et al., Indium tin oxide thin film deposition by magnetron sputtering at room temperature for the manufacturing of efficient transparent heaters. Coatings **11**(1), 92 (2021)
4. C.-S. Yang et al., Voltage-controlled liquid-crystal terahertz phase shifter with indium–tin–oxide nanowhiskers as transparent electrodes. Opt. Lett. **39**(8), 2511 (2014)
5. C.C. Wu, Highly flexible touch screen panel fabricated with silver-inserted transparent ITO triple-layer structures. R. Soc. Chem. **8**, 11862–11870 (2018)
6. T. Minami, Transparent conducting oxide semiconductors for transparent electrodes. Semiconduct. Sci. Technol. **20**(4), S35–S444 (2005)
7. B.G. Lewis, D.C. Paine, Applications and processing of transparent conducting oxides. Transp. Conduct. Oxides **25**(8), 22–27 (2000)
8. M. Mirzaee, A. Dolati, Effect of Cr doping on the structural, morphological, optical and electrical properties of indium tin oxide films. Appl. Phys. A **118**(3), 953–960 (2015)
9. S. Mohammadi, H. Abdizadeh, M.R. Golobostanfard, Opto-electronic properties of molybdenum doped indium tin oxide nanostructured thin films prepared via sol–gel spin coating. Ceram. Int. **39**(6), 6953–6961 (2013)
10. H. Taha et al., Improving the optoelectronic properties of titanium-doped indium tin oxide thin films. Semiconduct. Sci. Technol. **32**, 1361–6641 (2017)

11. C.-M. Hsu et al., Preparation and characterization of Ni–indium tin oxide cosputtered thin films for organic light-emitting diode application. Thin Solid Films **474**, 19–24 (2005)
12. B. Zhang et al., Characteristics of zirconium-doped indium tin oxide thin films deposited by magnetron sputtering. Sol. Energy Mater. Sol. Cells **92**(10), 1224–1229 (2008)
13. M. Mirzaee, A. Dolati, Effect of content silver and heat treatment temperature on morphological, optical, and electrical properties of ITO films by sol–gel technique. J. Nanopart. Res. **16**(8), 2585 (2014)
14. J. Philip et al., Carrier-controlled ferromagnetism in transparent oxide semiconductors. Nat. Mater. **5**(4), 298–304 (2006)
15. P. Alippi, M. Cesaria, V. Fiorentini, Impurity-vacancy complexes and ferromagnetism in doped sesquioxides. Phys. Rev. B **89**(13), 134423 (2014)
16. W.-C. Chang et al., Opto-electronic properties of chromium doped indium–tin-oxide films deposited at room temperature. Mater. Sci. Eng. B **153**(1–3), 57–61 (2008)
17. A. Caricato et al., Electrical and optical properties of ITO and ITO/Cr-doped ITO films. Appl. Phys. A **101**(4), 753–758 (2010)
18. C. Kim et al., A highly efficient indium tin oxide nanoparticles (ITO-NPs) transparent heater based on solution-process optimized with oxygen vacancy control. J. Alloy. Compd. **726**, 712–719 (2017)
19. H.-C. Lee, O.O. Park, Electron scattering mechanisms in indium-tin-oxide thin films: grain boundary and ionized impurity scattering. Vacuum **75**(3), 275–282 (2004)
20. D.-S. Liu et al., Thermal stability of indium tin oxide thin films co-sputtered with zinc oxide. Thin Solid Films **516**(10), 3196–3203 (2008)
21. J. Gwamuri et al., Influence of oxygen concentration on the performance of ultra-thin RF magnetron sputter deposited indium tin oxide films as a top electrode for photovoltaic devices. Materials **9**(1), 63 (2016)
22. S.J. Oh et al., Unveiling the annealing-dependent mechanical properties of freestanding indium tin oxide thin films. ACS Appl. Mater. Interfaces. **13**(14), 16650–16659 (2021)
23. R. Ali et al., Effects of residual stress distribution on interfacial adhesion of magnetron sputtered AlN and AlN/Al nanostructured coatings on a (100) silicon substrate. Nanomaterials **8**(11), 896 (2018)
24. R.D. Shannon, C.T. Prewitt, Effective ionic radii in oxides and fluorides. Acta Crystallogr. B **25**, 925 (1969)
25. M. Cesaria et al., Structural characterization of ultrathin Cr-doped ITO layers deposited by double-target pulsed laser ablation. J. Phys. D Appl. Phys. **44**(36), 365403 (2011)
26. R. Ali, M. Sebastiani, E. Bemporad, Influence of Ti–TiN multilayer PVD-coatings design on residual stresses and adhesion. Mater. Des. **75**, 47–56 (2015)
27. S. Thongmee et al., FePt films fabricated by electrodeposition. J. Appl. Phys. **101**(9), 09K519 (2007)
28. J.D. Bryan, D.R. Gamelin, Doped semiconductor nanocrystals: synthesis, characterization, physical properties, and applications. Prog. Inorg. Chem **54**(47), 47–126 (2005)
29. A. Sofi, M. Shah, K. Asokan, Structural, optical and electrical properties of ITO thin films. J. Electron. Mater. **47**(2), 1344–1352 (2018)
30. S.-K. Choi, J. Lee, Effect of film density on electrical properties of indium tin oxide films deposited by dc magnetron reactive sputtering. J. Vac. Sci. Technol. A: Vac. Surf. Films **19**(5), 2043–2047 (2001)
31. B. Pujilaksono et al., X-ray photoelectron spectroscopy studies of indium tin oxide nanocrystalline powder. Mater. Charact. **54**(1), 1–7 (2005)
32. H.S. Kim et al., Observation of ferromagnetism and anomalous Hall effect in laser-deposited chromium-doped indium tin oxide films. Solid State Commun. **137**(1–2), 41–43 (2006)
33. N.M. Ahmed et al., The effect of post annealing temperature on grain size of indium-tin-oxide for optical and electrical properties improvement. Results Phys. **13**, 102159 (2019)
34. P. Prepelita et al., Rapid thermal annealing for high-quality ITO thin films deposited by radio-frequency magnetron sputtering. Beilstein J. Nanotechnol. **10**(1), 1511–1522 (2019)
35. M. Cesaria et al., Optical analysis of Cr-doped ITO films deposited by double-target laser ablation. J. Lumin. **162**, 155–163 (2015)